J. Plasma Phys. (2025), *vol*. 91, E1
Published by Cambridge University Press

doi:10.1017/S0022377824001272

Stability analysis of partially ionized plasma in a porous medium with local thermal non-equilibrium effects

Vishal Chandel [1],† **and Sunil** [1]

[1]Department of Mathematics and Scientific Computing, National Institute of Technology Hamirpur, Hamirpur 177005, India

(Received 23 July 2024; revised 13 September 2024; accepted 23 September 2024)

This study investigates the impact of local thermal non-equilibrium on the stability analysis of partially ionized plasma within a porous medium. The plasma, heated from below, is enclosed by various combinations of bounding surfaces. Both nonlinear (via the energy method) and linear (utilizing the normal mode analysis method) analyses are performed. Eigenvalue problems for both analyses are formulated and solved using the Galerkin method. The study also explores the effects of compressibility, medium permeability and magnetic fields on system stability. The collisional frequency among plasma components and the thermal diffusivity ratio significantly influence energy decay. The results reveal that the Rayleigh–Darcy number is identical for both nonlinear and linear analyses, thus eliminating the possibility of a subcritical region and confirming global stability. The principle of exchange of stabilities is validated, indicating the absence of oscillatory convection modes. Medium permeability, heat-transfer coefficient and compressibility delay the onset of convection, demonstrating stabilizing effects. Conversely, the porosity-modified conductivity ratio hastens the convection process, indicating destabilizing effects. Rigid–rigid bounding surfaces are found to be thermally more stable for confining the partially ionized plasma. Additionally, the magnetic field exerts a stabilizing influence.

Key words: plasma dynamics, plasma instabilities, plasma heating

1. Introduction

Plasma, often called the fourth state of matter, stands apart from solids, liquids and gases due to its unique properties. The transition from solid to liquid to gas occurs with increasing heat, further heating of gas at sufficiently high temperatures causes its atoms to ionize, shedding the outermost electrons and resulting in a mix of positively charged ions and negatively charged electrons, known as plasma (Krishan 2022). Plasma can exist in various forms, categorized by the degree of ionization, with partially ionized plasma (PIP) consisting of both neutral and charged particles. Unlike fully ionized plasma, where nearly all particles are ionized, PIP allows for varied degrees of ionization depending on conditions and plasma source characteristics (Ballai 2019). In

† Email address for correspondence: vcvishal1950chandel@gmail.com

astrophysical contexts such as molecular clouds and the solar atmosphere, PIP plays a crucial role, with significant implications for understanding phenomena like solar flares and cometary tails (Ballester *et al.* 2018; Soler & Ballester 2022). These environments exhibit varying ionization levels, influencing electromagnetic processes and the plasma dynamics (Krishan 2022). Conversely, technological applications harness highly ionized plasmas in devices such as fusion reactors and plasma TVs. Several types of fluid instabilities, including Kelvin–Helmholtz, Rayleigh–Taylor, thermal and thermosolutal instabilities, are influenced by partial ionization effects (Soler & Ballester 2022). The study of PIP extends into diverse fields, including atmospheric science, plasma technology, laboratory research and astrophysics, owing to its complex behaviour and wide-ranging applications (Ballester *et al.* 2021; Kumar *et al.* 2021).

Thermal convection, a fundamental process in fluid dynamics, occurs when a fluid is heated from below, leading to a less dense lower layer than the upper layer, resulting in an unstable, top-heavy configuration. When the temperature difference or the depth of the layers overcomes the effect of gravity, the fluid ascends, revealing a cellular structure. This phenomenon, known as Bénard convection, is a significant topic in fluid dynamics and is thoroughly examined in Chandrasekhar's monograph (Chandrasekhar 1981). Thermal convection is crucial in various astronomical, natural and industrial processes, including atmospheric circulation, ocean flow and industrial heat transfer (Maheshwari & Bhatia 1976; Kaothekar 2018). Numerous studies have investigated thermal convection, contributing to our understanding of this complex phenomenon (Sharma 1972; Maheshwari & Bhatia 1976; Sharma & Sharma 1978, 1989; Sharma & Sunil 1995, 1996; Kaothekar 2018; Chandel & Sunil 2024; Chandel, Sunil & Sharma 2024; Mahajan & Raj 2024; Sharma, Sunil & Sharma 2024; Thakur, Kumar & Devi 2024).

The phenomenon of thermal convection within porous media has numerous real-world applications, such as in oil reservoir modelling, geothermal energy utilization, building thermal insulation, food processing and nuclear water disposal (Malashetty, Swamy & Kulkarni 2007; Shivakumara *et al.* 2011). The instability of a horizontal fluid-saturated porous layer when heated from below has been extensively researched and the growing volume of work devoted to this area is well documented by Straughan (2008) and Nield & Bejan (2013). A porous medium is a material containing pores (voids), where thermal convection occurs as fluid moves through these pores under a temperature gradient. In their study on the nonlinear stability of a rotating porous layer, Qin & Kaloni (1995) noted that, for highly porous materials, the Brinkman model, which accounts for the boundary layer effect, is superior to the Darcy model. This enhanced understanding of thermal convection in porous media underscores its significance in both theoretical exploration and practical applications, contributing to advancements across various scientific and industrial domains.

Studies on thermal convection in porous media heated from below often assume local thermal equilibrium (LTE), where the temperature gradient between fluid and solid phases is negligible at any location (Kuznetsov 1998; Malashetty *et al.* 2007). However, in many practical applications involving high-speed flows or substantial temperature differences between the fluid and solid phases, the LTE assumption proves inadequate (Kuznetsov 1998; Malashetty *et al.* 2007). In such scenarios, it is crucial to consider local thermal non-equilibrium (LTNE) effects by employing a two-field model for the energy equation, with separate representations for the fluid and solid phases (Kuznetsov 1998). Local thermal non-equilibrium theory finds particular relevance in diverse applications such as food drying, freezing processes, microwave heating, rapid heat transfer in computer chips utilizing porous metal foams and heat pipe technology (Malashetty *et al.* 2007;

https://doi.org/10.1017/S0022377824001272 Published online by Cambridge University Press

Shivakumara *et al.* 2011). These applications highlight the pivotal role LTNE theory is expected to play in future advancements.

Recent investigations have been dedicated to examining the effects of LTNE on forced and free convection in porous media. Comprehensive reviews of this research can be found in the works authored by Ingham & Pop (2005), Straughan (2008) and Nield & Bejan (2013). Kuznetsov (1998) provides detailed information about thermal non-equilibrium effects on internal forced convection flows. Postelnicu & Rees (2003) and Postelnicu (2008) examined convection onset using a thermal non-equilibrium model, focusing on stress-free and isothermal rigid boundaries. Rees & Pop (2005) offer an excellent review of research on LTNE phenomena in porous medium convection, primarily free and forced convection boundary layers and free convection within cavities. Straughan (2006) considered thermal convection in a fluid-saturated porous layer using a global nonlinear stability analysis with a thermal non-equilibrium model, establishing the equivalence of linear instability and nonlinear stability boundaries for thermal convection in a rotating porous layer with the Darcy law. Malashetty, Swamy & Heera (2008) studied double-diffusive convection in a fluid-saturated porous medium when the fluid and solid phases are not in LTE, using both linear and nonlinear stability analyses. Sunil, Sharma & Mahajan (2010) conducted an energy stability analysis of thermo-convective magnetized ferrofluid in a porous medium under thermal non-equilibrium conditions. Shivakumara *et al.* (2011) explored the effects of boundary and LTNE on the onset of convection in a sparsely packed horizontal anisotropic porous layer. Yadav & Lee (2015) investigated the onset of nanofluid convection in a rotating porous layer with zero nanoparticle flux boundary conditions under LTNE effects. Bansal & Suthar (2022) and Bansal & Suthar (2024) studied temperature modulation effects on Darcy–Bénard convection using the LTNE model. Arnone, Capone & Gianfrani (2024) have studied the stability of penetrative convection in a Darcy–Brinkman porous medium under the hypothesis of thermal non-equilibrium.

Despite extensive research, the field remains in a much-to-be-desired state, particularly regarding the effect of LTNE on the stability of a layer of PIP saturating a porous medium. To the best knowledge of the authors, no work has yet addressed this specific problem. Investigating the impact of LTNE on the stability of PIP heated from below is crucial for improving modelling accuracy and understanding plasma stability. Such insights are pivotal for applications in astrophysics, fusion research and various industrial sectors, including spacecraft propulsion, medical technologies and environmental sciences, thereby fostering scientific and practical advancements. Given the significance and identified gaps in the literature, in this study, we undertake both nonlinear and linear analyses to explore the LTNE effect on thermal convection in compressible PIP within a porous medium enclosed by various combinations of bounding surfaces. Linear analysis is examined using the normal mode analysis method (Chandrasekhar 1981), while nonlinear analysis employs the energy method (Straughan 2004, 2008). For numerical analysis, the Galerkin method (Yadav, Bhargava & Agarwal 2013) has been employed.

The paper is structured as follows: § 2 outlines the physical problem and presents the governing equations. In § 3, we solve the governing equations for the basic state, assuming the flow to be quiescent, and introduce perturbations to the system, deriving the non-dimensional perturbation equations. Section 4 is dedicated to nonlinear analysis, including the energy decay and the formulation of the eigenvalue problem for nonlinear analysis. In § 5, we focus on linear analysis and prove the principle of exchange of stability. Section 6 details the numerical methods for solving eigenvalue problems and provides expressions for the Rayleigh–Darcy number for various bounding surface configurations. Section 7 presents the results in graphical form and discusses the outcomes in detail.

https://doi.org/10.1017/S0022377824001272 Published online by Cambridge University Press

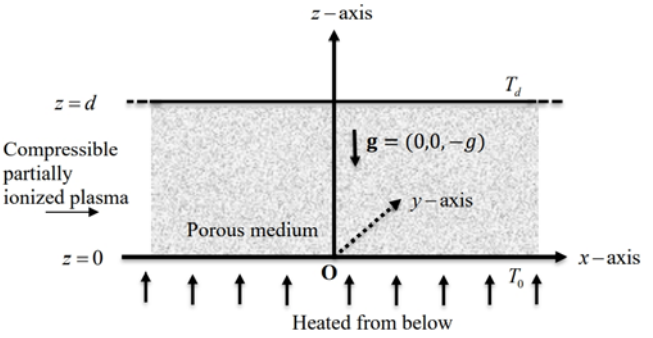

FIGURE 1. Geometrical representation of the problem.

Section 8 explores magnetic field effects. Finally, § 9 summarizes the major outcomes of our work.

2. Problem formulation

Consider an infinite horizontal layer of porous material saturated with compressible PIP, heated from below and confined between two surfaces at $z = 0$ and $z = d$. Let ρ_n denote the density of the neutral components of PIP, ρ_i the density of the ionized components of PIP and K_1 the permeability of the porous medium. The gravitational force, $\boldsymbol{g} = (0, 0, -g)$, acts downward. A geometrical representation of the problem is illustrated in figure 1.

We assume that the solid phase of the porous medium and the ionized components of the PIP are not in LTE. The temperature of the solid phase, T_s, and the plasma phase, T_i, are maintained constant at the surfaces $z = 0$ and $z = d$

$$T_s = T_i = T_0, \quad \text{at } z = 0 \quad \text{and} \quad T_s = T_i = T_d, \quad \text{at } z = d, \tag{2.1a,b}$$

where $T_0 > T_d$. A two-field model is employed to separately represent the temperature fields of the solid phase of the porous medium and the ionized components of the PIP in the energy equation.

In this analysis, the PIP is treated under the continuum hypothesis, behaving as a continuous fluid. Effects of LTNE, pressure, gravity and medium permeability on the neutral components of the PIP are considered negligibly small and are thus neglected.

Assuming adherence to the Boussinesq approximation (Spiegel & Veronis 1960), the governing equations are (cf. Sharma & Sharma 1978; Kuznetsov 1998; Straughan 2006; Nield & Bejan 2013)

$$\frac{1}{\epsilon}\frac{\partial \boldsymbol{q}}{\partial t} = -\frac{1}{\rho_m}\boldsymbol{\nabla} p + \boldsymbol{g}\left[1 - \alpha_m (T - T_m) + K_m (p - p_m)\right] - \frac{1}{\rho_m}\left[\frac{\mu}{K_1} - \tilde{\mu}\nabla^2\right]\boldsymbol{q} + \frac{\rho_d \nu_c}{\rho_m \epsilon}\left(\boldsymbol{q}_d - \boldsymbol{q}\right), \tag{2.2}$$

$$\epsilon\frac{\partial \rho}{\partial t} + (\boldsymbol{q}\cdot\boldsymbol{\nabla})\,\rho + \rho\boldsymbol{\nabla}\cdot\boldsymbol{q} = 0, \tag{2.3}$$

$$\epsilon\,(\rho c)_i\frac{\partial T_i}{\partial t} + (\rho c)_i\,(\boldsymbol{q}\cdot\boldsymbol{\nabla})\,T_i + p\boldsymbol{\nabla}\cdot\boldsymbol{q} = \epsilon k_i \nabla^2 T_i + h\,(T_s - T_i)\,, \tag{2.4}$$

https://doi.org/10.1017/S0022377824001272 Published online by Cambridge University Press

$$(1-\epsilon)\,(\rho c)_s\,\frac{\partial T_s}{\partial t} = (1-\epsilon)\,k_s\nabla^2 T_s - h\,(T_s - T_i)\,, \tag{2.5}$$

$$\frac{\partial \boldsymbol{q}_d}{\partial t} + \frac{1}{\epsilon}(\boldsymbol{q}_d \cdot \nabla)\boldsymbol{q}_d = -\nu_c(\boldsymbol{q}_d - \boldsymbol{q}). \tag{2.6}$$

Here, ϵ is the porosity, $\boldsymbol{q} = (u, v, w)$ and $\boldsymbol{q}_d = (\ell, r, s)$ are the velocities of the ionized and neutral components of PIP, respectively, t is time, p is pressure, ρ_m, T_m and p_m are the constant space averages of density, temperature and pressure, respectively, $\tilde{\mu}$ is the effective viscosity of PIP, μ is the dynamic viscosity of PIP, ν_c is the collisional frequency between components of PIP, k_i is the thermal conductivity of ionized components of PIP, h is the inter-phase heat transfer coefficient, c_i and c_s are the specific heats of the ionized components of the PIP and the solid phase of the porous medium, respectively, and k_s is the thermal conductivity of the solid phase of the porous medium. In (2.4) and (2.5), $(\rho c)_i = \rho_i c_i$ and $(\rho c)_s = \rho_s c_s$.

Additionally, α_m and K_m are defined as

$$\alpha_m = -\left(\frac{1}{\rho}\frac{\partial \rho}{\partial t}\right)_m (= \alpha, say)\,, \quad K_m = \left(\frac{1}{\rho}\frac{\partial \rho}{\partial p}\right)_m, \tag{2.7a,b}$$

where α is the coefficient of thermal expansion.

3. Basic state and non-dimensionalized perturbed equations

The steady basic state (Sharma & Sunil 1995) is defined as follows:

$$\boldsymbol{q} = \boldsymbol{q}_b = \boldsymbol{0}, \quad p = p_b\,(z)\,, \quad T_i = T_{i_b}\,(z)\,, \quad T_s = T_{s_b}\,(z) \quad \text{and} \quad \boldsymbol{q}_d = \boldsymbol{q}_{d_b} = \boldsymbol{0}, \tag{3.1a–e}$$

where

$$\left.\begin{aligned} \frac{1}{\rho_m}\nabla p_b\,(z) &= \boldsymbol{g}\left[1 - \alpha_m(T - T_m) + K_m\,(p - p_m)\right], \\ T_{i_b}\,(z) &= -\beta z + T_m = T_{s_b}\,(z)\,. \end{aligned}\right\} \tag{3.2}$$

Here, the subscript 'b' denotes the basic state and $\beta(= (T_0 - T_d)/d)$ is the temperature gradient.

Consider small disturbances in the form of

$$\boldsymbol{q}' = \left(u', v', w'\right), \quad p', \quad \boldsymbol{q}_d' = \left(\ell', r', s'\right), \quad \theta, \quad \text{and} \quad \psi, \tag{3.3a–e}$$

representing perturbations in $\boldsymbol{q}$, p, $\boldsymbol{q}_d$, T_i and T_s, respectively. The nonlinear perturbation equations are

$$\frac{1}{\epsilon}\frac{\partial \boldsymbol{q}'}{\partial t} = -\frac{1}{\rho_m}\nabla p' - \boldsymbol{g}\alpha\theta - \frac{1}{\rho_m}\left[\frac{\mu}{K_1} - \tilde{\mu}\nabla^2\right]\boldsymbol{q}' + \frac{\rho_d \nu_c}{\rho_m \epsilon}\left(\boldsymbol{q}_d' - \boldsymbol{q}'\right), \tag{3.4}$$

$$\nabla \cdot \boldsymbol{q}' = 0, \tag{3.5}$$

$$\epsilon\,(\rho c)_i\,\frac{\partial \theta}{\partial t} + (\rho c)_i\left(\boldsymbol{q}' \cdot \nabla\right)\theta = \epsilon k_i \nabla^2 \theta + h\,(\psi - \theta) + (\rho c)_i\left(\beta - \frac{g}{c_i}\right)w', \tag{3.6}$$

https://doi.org/10.1017/S0022377824001272 Published online by Cambridge University Press

$$(1-\epsilon)(\rho c)_s \frac{\partial \psi}{\partial t} = (1-\epsilon) k_s \nabla^2 \psi - h(\psi - \theta), \tag{3.7}$$

$$\frac{\partial \boldsymbol{q}_d'}{\partial t} + \frac{1}{\epsilon}\left(\boldsymbol{q}_d' \cdot \boldsymbol{\nabla}\right)\boldsymbol{q}_d' = -\nu_c\left(\boldsymbol{q}_d' - \boldsymbol{q}'\right). \tag{3.8}$$

The perturbed equations (3.4)–(3.8) are non-dimensionalized using the following scales:

$$\left.\begin{aligned} t^* = \frac{k_i}{d^2(\rho c)_i} t, \quad \boldsymbol{q}^* = \frac{(\rho c)_i d}{\epsilon k_i}\boldsymbol{q}', \quad \boldsymbol{q}_d^* = \frac{(\rho c)_i d}{\epsilon k_i}\boldsymbol{q}_d', \quad z^* = \frac{z}{d}, \\ p^* = \frac{K_1(\rho c)_i}{\mu \epsilon k_i} p^*, \quad \theta^* = \frac{\sqrt{Ra}}{\beta d}\theta, \quad \psi^* = \frac{\sqrt{Ra}}{\beta d}\psi. \end{aligned}\right\} \tag{3.9}$$

As a result, the non-dimensionalized perturbed equations (after removing the asterisk) are given as

$$\frac{1}{Va}\frac{\partial \boldsymbol{q}}{\partial t} = -\boldsymbol{\nabla} p + \sqrt{Ra}\theta \hat{\boldsymbol{k}} - \boldsymbol{q} + \widetilde{Da}\nabla^2 \boldsymbol{q} + \frac{FLPr}{Va}\left(\boldsymbol{q}_d - \boldsymbol{q}\right), \tag{3.10}$$

$$\boldsymbol{\nabla} \cdot \boldsymbol{q} = 0, \tag{3.11}$$

$$\frac{\partial \theta}{\partial t} + (\boldsymbol{q} \cdot \boldsymbol{\nabla})\theta = \nabla^2 \theta + \mathcal{H}(\psi - \theta) + \sqrt{Ra}\left(1 - \frac{1}{G}\right) w, \tag{3.12}$$

$$\mathcal{A}\frac{\partial \psi}{\partial t} = \nabla^2 \psi - \mathcal{H}\gamma(\psi - \theta), \tag{3.13}$$

$$\frac{\partial \boldsymbol{q}_d}{\partial t} + \left(\boldsymbol{q}_d \cdot \boldsymbol{\nabla}\right)\boldsymbol{q}_d = -LPr\left(\boldsymbol{q}_d - \boldsymbol{q}\right). \tag{3.14}$$

Here, $Va = (\rho c)_i d^2 \mu \epsilon / k_i \rho_m K_1$ is the Vadasz number, $Ra = g\alpha\beta d^2 K_1 \rho_m (\rho c)_i / \mu \epsilon k_i$ is the Rayleigh–Darcy number, $\widetilde{Da} = \tilde{\mu} K_1 / \mu d^2$ is the Darcy–Brinkman number, $L = \nu_c d^2 \rho_m / \mu$ is the collisional frequency parameter of PIP, $Pr = \mu(\rho c)_i / k_i \rho_m$ is the Prandtl number, $F = \rho_n / \rho_m$ is the ratio of densities of neutral to ionized components of PIP, $\mathcal{H} = hd^2/\epsilon k_i$ is the scaled inter-phase heat-transfer coefficient, $G = g\rho_m/(\rho c)_i \beta$ is the compressibility parameter, $\mathcal{A} = (\rho c)_s k_i / (\rho c)_i K_s$ is the diffusivity ratio and $\gamma = \epsilon k_i / (1-\epsilon) k_s$ is the porosity-modified conductivity ratio.

To investigate the impact of the collisional frequency of two components of PIP on the system's stability, we neglect the convective term in (3.14) as it is independent of the collisional frequency. Subsequently, using the normal mode analysis technique on (3.14), we obtain

$$\boldsymbol{q}_d = \left(\frac{PrL}{n + L}\right)\boldsymbol{q}, \tag{3.15}$$

where $n(\equiv \partial/\partial t)$ is the frequency of harmonic disturbances (Sharma & Sharma 1978). Substituting (3.15) into (3.10), we get

$$\frac{1}{Va}\left[1 + \frac{FLPr}{n + LPr}\right]\frac{\partial \boldsymbol{q}}{\partial t} = -\boldsymbol{\nabla} p + \sqrt{Ra}\theta \hat{\boldsymbol{k}} - \boldsymbol{q} + \widetilde{Da}\nabla^2 \boldsymbol{q}. \tag{3.16}$$

The boundary conditions (BCs) associated with (3.11)–(3.13) and (3.16) are

$$\boldsymbol{q} = \boldsymbol{0}, \quad \theta = 0, \quad \psi = 0 \quad \text{on } z = 0, 1, \tag{3.17}$$

and plane tiling periodicity in x and y is satisfied by $\boldsymbol{q}$, θ and ψ (Straughan 2006).

https://doi.org/10.1017/S0022377824001272 Published online by Cambridge University Press

4. Nonlinear analysis

To perform a nonlinear analysis, we employ the energy method. Let $\|\cdot\|$ denote the $L^2(V)$ norm, $\langle\cdot\rangle$ denote integration over V and V denote the three-dimensional periodicity cell. To begin, multiply (3.16) by $\boldsymbol{q}$, (3.12) by θ and (3.13) by ψ/γ. Integrating the resulting equations over V and using (3.11) and the BCs, we obtain

$$\frac{1}{2Va}\left[1+\frac{FLPr}{n+LPr}\right]\frac{\mathrm{d}}{\mathrm{d}t}\|\boldsymbol{q}\|^2=\sqrt{Ra}\langle w\theta\rangle-\|\boldsymbol{q}\|^2-\widetilde{Da}\,\|\nabla\boldsymbol{q}\|^2\,, \tag{4.1}$$

$$\frac{1}{2}\frac{\mathrm{d}}{\mathrm{d}t}\|\theta\|^2=\sqrt{Ra}\left(1-\frac{1}{G}\right)\langle w\theta\rangle-\mathcal{H}\langle\theta\,(\theta-\psi)\rangle-\|\nabla\theta\|^2\,, \tag{4.2}$$

$$\frac{\mathcal{A}}{2\gamma}\frac{\mathrm{d}}{\mathrm{d}t}\|\psi\|^2=-\mathcal{H}\langle\psi\,(\psi-\theta)\rangle-\frac{1}{\gamma}\|\nabla\psi\|^2\,. \tag{4.3}$$

By adding (4.1)–(4.3), we get

$$\frac{\mathrm{d}E}{\mathrm{d}t}=I_0-D_0, \tag{4.4}$$

where $E(t)$ is energy, I_0 is the production term and D_0 is the dissipation term. Here,

$$E(t)=\frac{1}{2}\|\theta\|^2+\frac{\lambda}{2Va}\left[1+\frac{FLPr}{n+LPr}\right]\|\boldsymbol{q}\|^2+\frac{\mathcal{A}}{2\gamma}\|\psi\|^2\,, \tag{4.5}$$

$$I_0=\lambda\sqrt{Ra}\langle w\theta\rangle+\sqrt{Ra}\left(1-\frac{1}{G}\right)\langle w\theta\rangle, \tag{4.6}$$

$$D_0=\lambda\left(\widetilde{Da}\,\|\nabla\boldsymbol{q}\|^2+\|\boldsymbol{q}\|^2\right)+\|\nabla\theta\|^2+\mathcal{H}\,\|\theta-\psi\|^2+\frac{1}{\gamma}\|\nabla\psi\|^2\,, \tag{4.7}$$

where λ is the coupling parameter.

From (4.4), we obtain

$$\frac{\mathrm{d}E}{\mathrm{d}t}\leqslant(m-1)\,D_0, \tag{4.8}$$

where

$$m=\max_{\mathcal{G}}\frac{I_0}{D_0}, \tag{4.9}$$

and $\mathcal{G}$ is the admissible solution space.

Using the Poincaré inequality, (4.7) becomes

$$D_0\geqslant K^*E(t), \tag{4.10}$$

where

$$K^*=2\pi^2\min\left\{1,\frac{1}{\mathcal{A}},\frac{1}{Va}\left(\frac{1}{\pi^2}+\widetilde{Da}\right)\left[1+\frac{FLPr}{n+LPr}\right]^{-1}\right\}. \tag{4.11}$$

Using inequality (4.10) in inequality (4.8), we get

$$\frac{\mathrm{d}E}{\mathrm{d}t}\leqslant-a_0K^*E(t), \tag{4.12}$$

where $a_0=1-m>0$.

https://doi.org/10.1017/S0022377824001272 Published online by Cambridge University Press

By integrating inequality (4.12), we get

$$E(t) \leqslant E(0)\exp(-a_o K^* t). \tag{4.13}$$

From inequality (4.13), it follows that $E(t) \to 0$ exponentially as $t \to \infty$. This ensures the stability for all values of $E(0)$. The collisional frequency plays a significant role in energy decay, particularly when

$$\left\{1, \frac{1}{\mathcal{A}}\right\} > \frac{1}{Va}\left(\frac{1}{\pi^2} + \widetilde{Da}\right)\left[1 + \frac{FLPr}{n + LPr}\right]^{-1}. \tag{4.14}$$

Similarly, the thermal diffusivity ratio is important if

$$\left\{1, \frac{1}{Va}\left(\frac{1}{\pi^2} + \widetilde{Da}\right)\left[1 + \frac{FLPr}{n + LPr}\right]^{-1}\right\} > \frac{1}{\mathcal{A}}. \tag{4.15}$$

These conditions define thresholds where the collisional frequency and thermal diffusivity ratio significantly influence the stability and energy dynamics of the system under consideration.

4.1. *Eigenvalue problem for nonlinear analysis*

The value of Ra is calculated from the Euler–Lagrange equations derived from (4.9), namely

$$\frac{\sqrt{Ra}}{\sqrt{\lambda}}\left[\lambda + \frac{G-1}{G}\right]\theta - 2\boldsymbol{q} + 2\widetilde{Da}\nabla^2\boldsymbol{q} = 0, \tag{4.16}$$

$$\frac{\sqrt{Ra}}{\sqrt{\lambda}}\left[\lambda + \frac{G-1}{G}\right]w + 2\nabla^2\theta - 2\mathcal{H}(\theta - \psi) = 0, \tag{4.17}$$

$$\frac{2}{\gamma}\nabla^2\psi + 2\mathcal{H}(\theta - \psi) = 0. \tag{4.18}$$

Operating $\hat{\boldsymbol{k}} \cdot$ curlcurl on (4.16), we get

$$\frac{\sqrt{Ra}}{\sqrt{\lambda}}\left[\lambda + \frac{G-1}{G}\right]\nabla_1^2\theta - 2\nabla^2 w + 2\widetilde{Da}\nabla^4 w = 0, \tag{4.19}$$

where

$$\nabla_1^2 \equiv \frac{\partial^2}{\partial x^2} + \frac{\partial^2}{\partial y^2}. \tag{4.20}$$

We assume a plane tiling of the form

$$\{w, \theta, \psi\} = \{W(z), \Theta(z), \Psi(z)\}f(x, y), \tag{4.21}$$

where f is a planform satisfying $\nabla_1^2 f + a^2 f = 0$, a being a wavenumber.

https://doi.org/10.1017/S0022377824001272 Published online by Cambridge University Press

Using the plane form (4.21), (4.19), (4.17) and (4.18) become

$$\frac{\sqrt{Ra}}{\sqrt{\lambda}}\left[\lambda+\frac{G-1}{G}\right]a^2\Theta-2\widetilde{Da}\left(D^2-a^2\right)^2W+2\left(D^2-a^2\right)W=0, \tag{4.22}$$

$$\frac{\sqrt{Ra}}{\sqrt{\lambda}}\left[\lambda+\frac{G-1}{G}\right]W+2\left(D^2-a^2\right)\Theta-2\mathcal{H}\left(\Theta-\Psi\right)=0, \tag{4.23}$$

$$\frac{2}{\gamma}\left(D^2-a^2\right)\Psi+2\mathcal{H}\left(\Theta-\Psi\right)=0, \tag{4.24}$$

where $D=\mathrm{d}/\mathrm{d}z$. The BCs associated with (4.22)–(4.24) are

$$\left.\begin{array}{ll} W=\Psi=\Theta=0 & \text{for } z=0,\,1,\\ \text{and} \quad DW=0 & \text{for rigid surface,}\\ \text{and} \quad D^2W=0 & \text{for free surface.}\end{array}\right\} \tag{4.25}$$

The set of equations (4.22)–(4.24), together with the BCs (4.25), constitutes the eigenvalue problem for nonlinear analysis.

5. Linear analysis

To study the linear analysis, by considering the perturbation to be infinitesimally small, we ignore the nonlinear terms from the non-dimensional perturbed equations and obtain the linearized non-dimensional perturbed equations as

$$\frac{1}{Va}\left[1+\frac{FLPr}{n+LPr}\right]\frac{\partial \boldsymbol{q}}{\partial t}=-\boldsymbol{\nabla}p+\sqrt{Ra}\theta\hat{\boldsymbol{k}}-\boldsymbol{q}+\widetilde{Da}\nabla^2\boldsymbol{q}, \tag{5.1}$$

$$\frac{\partial\theta}{\partial t}=\sqrt{Ra}\left(1-\frac{1}{G}\right)w+\mathcal{H}\left(\psi-\theta\right)+\nabla^2\theta, \tag{5.2}$$

$$\mathcal{A}\frac{\partial\psi}{\partial t}=-\mathcal{H}\gamma\left(\psi-\theta\right)+\nabla^2\psi. \tag{5.3}$$

Operating $\hat{\boldsymbol{k}}\cdot$ curlcurl on (5.1), we get

$$\frac{1}{Va}\left[1+\frac{FLPr}{n+LPr}\right]\frac{\partial}{\partial t}\left(\nabla^2w\right)=\sqrt{Ra}\nabla_1^2\theta-\nabla^2w+\widetilde{Da}\nabla^4w. \tag{5.4}$$

By applying the normal mode analysis method to equations (5.4), (5.2) and (5.3), where we assumed the perturbed quantities of the form

$$\{w,\theta,\psi\}=\{W(z),\Theta(z),\Psi(z)\}\exp\left\{\iota\left(a_xx+a_yy\right)+nt\right\}. \tag{5.5}$$

Here, $\sqrt{a_x^2+a_y^2}=a$ is the wavenumber.

https://doi.org/10.1017/S0022377824001272 Published online by Cambridge University Press

Using (5.5), equations (5.4), (5.2) and (5.3) become

$$\frac{1}{Va}\left[1+\frac{FLPr}{n+LPr}\right]n\left(D^2-a^2\right)W=-\sqrt{Ra}a^2\Theta-\left(D^2-a^2\right)W+\widetilde{Da}\left(D^2-a^2\right)^2W, \tag{5.6}$$

$$n\Theta=\left(D^2-a^2\right)\Theta+\mathcal{H}\left(\Psi-\Theta\right)+\sqrt{Ra}\left(1-\frac{1}{G}\right)W, \tag{5.7}$$

$$\mathcal{A}n\Psi=\left(D^2-a^2\right)\Psi-\mathcal{H}\gamma\left(\Psi-\Theta\right). \tag{5.8}$$

The BCs associated with (5.6)–(5.8) are same as (4.25).

5.1. *Exchange of stabilities*

Here, we prove that the principle of exchange of stabilities is valid, namely that marginally stable modes with $\sigma=0$ also have $\omega=0$, where $\sigma+\iota\omega=n$.

Multiply (5.6) by W^* (complex conjugate of W), (5.7) by Θ^* (complex conjugate of Θ) and (5.8) by Ψ^* (complex conjugate of Ψ), integrating resulting equations over the range of z and using BCs (4.25), we get

$$-\frac{n}{Va}\left[1+\frac{FLPr}{n+LPr}\right]\mathcal{I}_1+\sqrt{Ra}a^2\int_0^1 W^*\Theta\,\mathrm{d}z-\mathcal{I}_1-\widetilde{Da}\mathcal{I}_2=0, \tag{5.9}$$

$$n\mathcal{I}_3+\mathcal{I}_4-\mathcal{H}\int_0^1\Theta^*\Psi\,\mathrm{d}z+\mathcal{H}\mathcal{I}_3-\sqrt{Ra}\left(1-\frac{1}{G}\right)\int_0^1 W\Theta^*\,\mathrm{d}z=0, \tag{5.10}$$

$$\mathcal{A}n\mathcal{I}_5+\mathcal{I}_6+\mathcal{H}\gamma\mathcal{I}_5-\mathcal{H}\gamma\int_0^1\Theta\Psi^*\,\mathrm{d}z, \tag{5.11}$$

where

$$\left.\begin{aligned}\mathcal{I}_1=\int_0^1\left(|DW|^2+a^2|W|^2\right)\mathrm{d}z,\quad \mathcal{I}_2=\int_0^1\left(|D^2W|^2+2a^2|DW|^2+a^4|W|^2\right)\mathrm{d}z,\\ \mathcal{I}_3=\int_0^1|\Theta|^2\,\mathrm{d}z,\quad \mathcal{I}_4=\int_0^1\left(|D\Theta|^2+a^2|\Theta|^2\right)\mathrm{d}z,\\ \mathcal{I}_5=\int_0^1|\Psi|^2\,\mathrm{d}z,\quad \mathcal{I}_6=\int_0^1\left(|D\Psi|^2+a^2|\Psi|^2\right)\mathrm{d}z.\end{aligned}\right\} \tag{5.12}$$

The integrals $\mathcal{I}_1$, $\mathcal{I}_2$, $\mathcal{I}_3$, $\mathcal{I}_4$, $\mathcal{I}_5$ and $\mathcal{I}_6$ are positive. So, subtracting the product of a^2 with (5.11) from the sum of the product of $(1-1/G)\gamma$ with (5.9) and the product of $a^2\gamma$ with complex conjugate of (5.10), we get

$$\begin{aligned}&-\gamma\left(1-\frac{1}{G}\right)\left(\frac{n}{Va}\left[1+\frac{FLPr}{n+LPr}\right]+1\right)\mathcal{I}_1-\left(1-\frac{1}{G}\right)\gamma\widetilde{Da}\mathcal{I}_2\\&+a^2\gamma\left(n^*+\mathcal{H}\right)\mathcal{I}_3+a^2\gamma\mathcal{I}_4-a^2\left(\mathcal{A}n+\gamma\mathcal{H}\right)\mathcal{I}_5-a^2\mathcal{I}_6=0,\end{aligned} \tag{5.13}$$

where n^* is the complex conjugate of n.

https://doi.org/10.1017/S0022377824001272 Published online by Cambridge University Press

The imaginary part of (5.13) gives

$$\omega\left\{\left(1-\frac{1}{G}\right)\left(\frac{1}{Va}+\frac{FL^2(Pr)^2}{(\sigma+LPr)^2+\omega^2}\right)\gamma\mathcal{I}_1+a^2\gamma\mathcal{I}_3+a^2\mathcal{A}\mathcal{I}_5\right\}=0. \tag{5.14}$$

The quantity inside the curly brackets is positive definite for G is greater than 1. Hence, (5.14) suggests that $\omega = 0$. This establishes that the principle of exchange of stabilities is valid (Chandrasekhar 1981).

Now, keeping in mind the validation of the principle of exchange of stabilities, (5.6)–(5.8) can be rewritten as

$$\sqrt{Ra}a^2\Theta+\left(D^2-a^2\right)W-\widetilde{Da}\left(D^2-a^2\right)^2W=0, \tag{5.15}$$

$$\left(D^2-a^2\right)\Theta+\mathcal{H}\left(\Psi-\Theta\right)+\sqrt{Ra}\left(1-\frac{1}{G}\right)W=0, \tag{5.16}$$

$$\left(D^2-a^2\right)\Psi-\mathcal{H}\gamma\left(\Psi-\Theta\right)=0. \tag{5.17}$$

The set of equations (5.15)–(5.17), together with the BCs (4.25), constitutes the eigenvalue problem for linear analysis.

6. Method of solution

The eigenvalue problems for both nonlinear as well as linear analyses have been solved using the single-term Galerkin method. In this method, the weighted functions are the same as the base (trial) functions (Yadav *et al.* 2013). Accordingly, we define W, Θ and Ψ in the following form:

$$W=\sum_{j=1}^{N}A_jW_j,\quad \Theta=\sum_{j=1}^{N}B_j\Theta_j,\quad \Psi=\sum_{j=1}^{N}C_j\Psi_j, \tag{6.1a-c}$$

where A_j, B_j and C_j are unknown coefficients, $j = 1, 2, 3, \ldots, N$ and the base functions W_j, Θ_j and Ψ_j are assumed to be in the following forms for free–free, rigid–free and rigid–rigid bounding surfaces (Chandrasekhar 1981; Yadav *et al.* 2013), respectively:

$$W_j=\sin(j\pi z)=\Theta_j=\Psi_j, \tag{6.2}$$

$$W_j=z^2\left(1-z\right)\left[(j+2)-2z^j\right],\quad \Theta_j=z^j-z^{j+1}=\Psi_j, \tag{6.3a,b}$$

$$W_j=z^{j+1}-2z^{j+2}+z^{j+3},\quad \Theta_j=z^j-z^{j+1}=\Psi_j, \tag{6.4a,b}$$

such that W_j, Θ_j and Ψ_j satisfy the corresponding BCs (4.25). By substituting the expressions for W, Θ and Ψ into (4.22)–(4.24) and (5.15)–(5.17), and then multiplying the first equation by W_j, the second equation by Θ_j and the third equation by Ψ_j and integrating the resulting equations over the interval from zero to unity, we obtain a set of linear homogeneous equations. This set of equations admits a non-trivial solution only if its determinant is equal to zero, which gives the characteristic equations of the eigenvalue problems in terms of the Rayleigh–Darcy number Ra.

https://doi.org/10.1017/S0022377824001272 Published online by Cambridge University Press

6.1. *Rayleigh–Darcy number for free–free bounding surfaces*

For nonlinear analysis, Ra has been found as a function of a, λ, $\mathcal{H}$, γ and G. The expression for Ra is given by

$$Ra = \frac{4G^2\left(a^2+\pi^2\right)^2\left(1+a^2\widetilde{Da}+\pi^2\widetilde{Da}\right)\left(a^2+\pi^2+\mathcal{H}+\gamma\mathcal{H}\right)\lambda}{a^2\left(a^2+\pi^2+\gamma\mathcal{H}\right)(G-1+G\lambda)^2}. \tag{6.5}$$

The optimal value of λ has been found using the condition $\mathrm{d}Ra/\mathrm{d}\lambda = 0$, which yields $\lambda = (G-1)/G$. Using this value, the expression for Ra becomes

$$Ra = \left(\frac{G}{G-1}\right)\frac{\left(a^2+\pi^2\right)^2\left(1+a^2\widetilde{Da}+\pi^2\widetilde{Da}\right)\left(a^2+\pi^2+\mathcal{H}+\gamma\mathcal{H}\right)}{a^2\left(a^2+\pi^2+\gamma\mathcal{H}\right)}. \tag{6.6}$$

For linear analysis, the value of Ra found by solving the eigenvalue problem (5.15)–(5.17) using the Galerkin method has been the same as (6.6).

6.2. *Rayleigh–Darcy number for rigid–free bounding surfaces*

For nonlinear analysis, Ra has been found as a function of a, λ, $\mathcal{H}$, γ and G. The expression for Ra is given by

$$Ra = \frac{112G^2\left(10+a^2\right)\left(19a^4\widetilde{Da}+216\left(1+21\widetilde{Da}\right)+a^2\left(19+432\widetilde{Da}\right)\right)\left(10+a^2+\mathcal{H}+\gamma\mathcal{H}\right)\lambda}{507a^2\left(10+a^2+\gamma\mathcal{H}\right)(G-1+G\lambda)^2}. \tag{6.7}$$

The optimal value of λ has been found using the condition $dRa/d\lambda = 0$, which yields $\lambda = (G-1)/G$. Using this value, the expression for Ra becomes

$$Ra = \frac{28G\left(10+a^2\right)\left(19a^4\widetilde{Da}+216\left(1+21\widetilde{Da}\right)+a^2\left(19+432\widetilde{Da}\right)\right)\left(10+a^2+\mathcal{H}+\gamma\mathcal{H}\right)}{507a^2(G-1)\left(10+a^2+\gamma\mathcal{H}\right)}. \tag{6.8}$$

For linear analysis, the value of Ra found by solving the eigenvalue problem (5.15)–(5.17) using the Galerkin method has been the same as (6.8).

6.3. *Rayleigh–Darcy number for rigid–rigid bounding surfaces*

For nonlinear analysis, Ra has been found as a function of a, λ, $\mathcal{H}$, γ and G. The expression for Ra is given by

$$Ra = \frac{112G^2\left(10+a^2\right)\left(12+504\widetilde{Da}+a^4\widetilde{Da}+a^2\left(1+24\widetilde{Da}\right)\right)\left(10+a^2+\mathcal{H}+\gamma\mathcal{H}\right)\lambda}{27a^2\left(10+a^2+\gamma\mathcal{H}\right)(G-1+G\lambda)^2}. \tag{6.9}$$

The optimal value of λ has been found using the condition $\mathrm{d}Ra/\mathrm{d}\lambda = 0$, which yields $\lambda = (G-1)/G$. Using this value, the expression for Ra becomes

$$Ra = \frac{28G\left(10+a^2\right)\left(12+504\widetilde{Da}+a^4\widetilde{Da}+a^2\left(1+24\widetilde{Da}\right)\right)\left(10+a^2+\mathcal{H}+\gamma\mathcal{H}\right)}{27a^2(G-1)\left(10+a^2+\gamma\mathcal{H}\right)}. \tag{6.10}$$

For linear analysis, the value of Ra found by solving the eigenvalue problem (5.15)–(5.17) using the Galerkin method has been the same as (6.10).

Here, Ra has the same value for both nonlinear and linear analyses, indicating a lack of subcritical regions and demonstrating strong global stability. It has been observed that collisional effects contribute to energy decay, but do not affect the value of Ra in either nonlinear or linear analyses.

https://doi.org/10.1017/S0022377824001272 Published online by Cambridge University Press

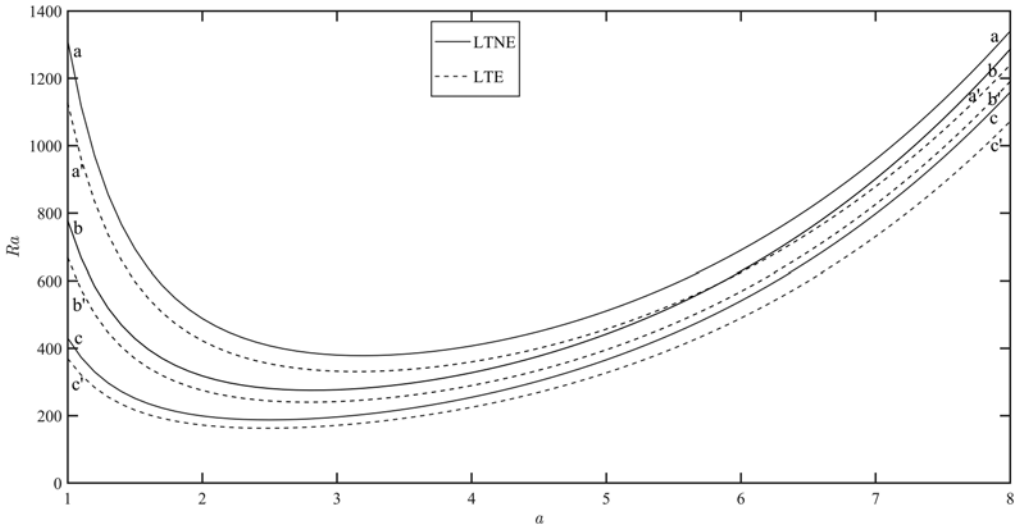

FIGURE 2. Comparison of Rayleigh–Darcy number (*Ra*) for LTNE and LTE across various combinations of bounding surfaces. Solid curves depict *Ra* variations for LTNE, while dotted curves show *Ra* variations for LTE. Curves labelled aa, bb and cc show the variations of *Ra* with wavenumber (a) for rigid–rigid, rigid–free and free–free surfaces, respectively, under LTNE conditions. The curves labelled a′a′, b′b′ and c′c′ represent the variations of *Ra* with a for rigid–rigid, rigid–free and free–free bounding surfaces, respectively, under LTE conditions.

7. Results and discussion

This section presents graphical representations of neutral stability curves for various parameter values. Numerical calculations are conducted with $G = 3$, $\widetilde{Da}$ ranging from 0 to 1, $\mathcal{H}$ ranging from 10^{-5} to 10^{5} and γ ranging from 0 to 10. The parameter ranges discussed are inspired by the existing literature (Sharma & Sunil 1995; Malashetty *et al.* 2007, 2008; Nield & Bejan 2013; Yadav & Lee 2015).

It is evident from the expressions of *Ra* that, as the values of G increase, *Ra* also increases, suggesting that compressibility exerts a stabilizing influence. Notably, cases where $G = 1$ and $G < 1$ are not applicable in this study, as they result in infinite or negative *Ra*. The significance of this relationship becomes particularly pronounced when G exceeds 1, as emphasized in a study by Sharma & Sunil (1995).

Figure 2 compares LTNE and LTE conditions for the distinct combinations of free and rigid bounding surfaces. The values of *Ra* for respective bounding surfaces have been calculated using $\mathcal{H} \to 0$ in (6.6), (6.8) and (6.10), for LTE conditions and for LTNE conditions using $\mathcal{H} = 10$ and $\gamma = 5$. The value of $\widetilde{Da}$ is kept fixed as 0.1 for both LTE and LTNE. It is clear from the figure that the values of *Ra* in the case of LTNE are more than that of the LTE case for respective bounding surfaces. This indicates that onset convection occurs earlier for the LTE conditions than for the LTNE conditions.

In figure 3, the variation of Ra_c with $\widetilde{Da}$ for different combinations of bounding surfaces at $\mathcal{H} = 100$, $\gamma = 5$ and $G = 3$ is displayed. This figure illustrates the stabilizing effect of medium permeability for all three different combinations of bounding surfaces. This behaviour occurs because permeability adds resistance to the flow of PIP, leading to enhanced mixing of PIP and more efficient temperature distribution. Consequently, the convective heat transfer increases, delaying the onset of convection and increasing Ra_c.

https://doi.org/10.1017/S0022377824001272 Published online by Cambridge University Press

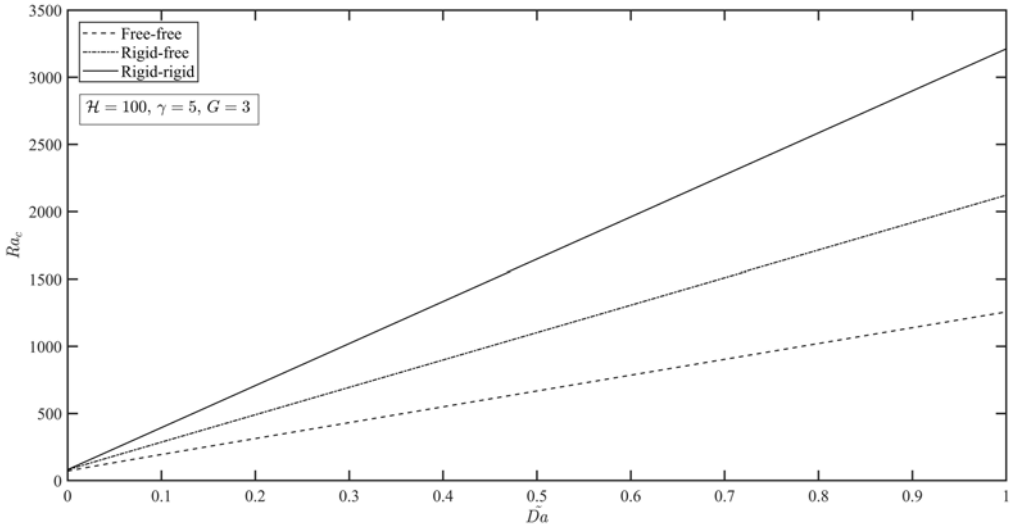

FIGURE 3. Variation of critical Rayleigh–Darcy number (Ra_c) with Darcy–Brinkman number ($\widetilde{Da}$) for the distinct combinations of bounding surfaces.

In figure 4, the relationship between Ra_c and the scaled inter-phase heat transfer coefficient ($\log_{10}\mathcal{H}$) for different bounding surface combinations is illustrated. It is observed that, as $\mathcal{H}$ increases, Ra_c also increases, indicating a stabilizing effect. For small $\mathcal{H}$ values, Ra_c shows minimal variation and is independent of γ. However, for $\mathcal{H} > 1$, the variation becomes significant as Ra_c becomes dependent on γ. This behaviour is a result of the negligible heat transfer between the phases at low $\mathcal{H}$ values, making the critical value unaffected by the solid phase properties. Conversely, at high $\mathcal{H}$ values, the temperatures of the phases nearly equalize, allowing them to be treated as a single phase. In between these extremes, $\mathcal{H}$ introduces strong non-equilibrium effects. Additionally, an increase in γ leads to a decrease in Ra_c, highlighting the destabilizing influence of γ. This trend is further illustrated in figure 5, which is plotted for a constant $\mathcal{H}$. Higher γ values imply that heat is transported through both the solid and PIP phases, whereas lower values indicate that heat is transported primarily through the PIP phase. Thus, convection is more readily initiated for higher γ values when all the other parameters are held constant.

Additionally, based on these graphical results, we infer that PIP exhibits greater thermal stability when confined between rigid–rigid bounding surfaces, while it shows less thermal stability when the plasma layer is confined between free–free bounding surfaces.

8. Effect of magnetic field

To study the effect of the magnetic field on the problem of instability described in § 2, we consider a horizontal porous layer of PIP, subjected to a magnetic field $\boldsymbol{H}$. We have adopted the quasi-static magnetohydrodynamic approximation proposed by Galdi & Straughan (1985). The key modification is to include a term representing the Lorentz force ($\boldsymbol{\mathcal{L}} = \boldsymbol{j} \times \boldsymbol{B}_0$) in the equation of motion (2.3), where $\boldsymbol{j}$ is the current and $\boldsymbol{B}_0 = (0, 0, B_0)$ is the magnetic field with only vertical component (Chandrasekhar 1981). The non-dimensional perturbed equations (3.11)–(3.13) remains the same but

https://doi.org/10.1017/S0022377824001272 Published online by Cambridge University Press

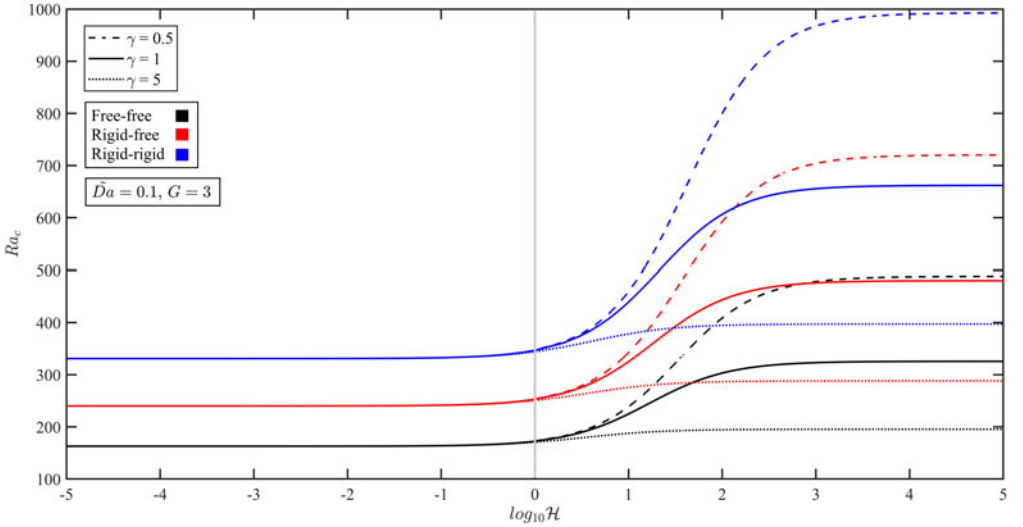

FIGURE 4. Comparison of critical Rayleigh–Darcy number (Ra_c) for various values of scaled inter-phase heat-transfer coefficient ($\log_{10}\mathcal{H}$), for different values of porosity-modified conductivity ratio (γ), for distinct combination of bounding surfaces. The blue curves represent rigid–rigid bounding surfaces, the red curves indicate rigid–free bounding surfaces and the black curves correspond to free–free bounding surfaces. The dashed curves are for $\gamma = 0.5$, the solid curves for $\gamma = 1$ and the dotted curves for $\gamma = 5$.

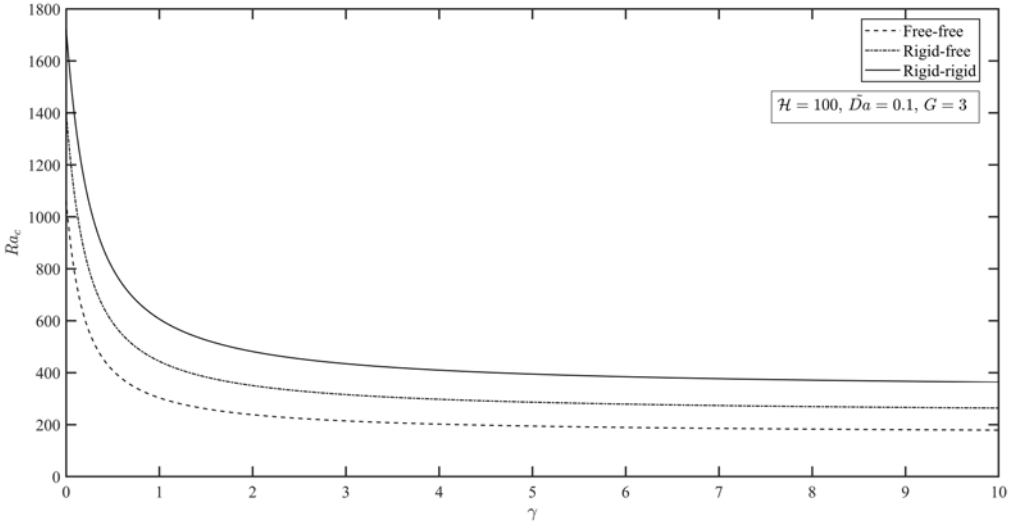

FIGURE 5. Variation of critical Rayleigh–Darcy number (Ra_c) with porosity-modified conductivity ratio (γ) for the distinct combinations of bounding surfaces.

(3.16) becomes

$$\frac{1}{Va}\left[1+\frac{FLPr}{n+LPr}\right]\frac{\partial \boldsymbol{q}}{\partial t} = -\nabla p + \sqrt{Ra}\theta\hat{\boldsymbol{k}} - \boldsymbol{q} + \widetilde{Da}\nabla^2\boldsymbol{q} + \frac{M^2\widetilde{Da}}{Vr}\left[\left(\boldsymbol{q}\times\hat{\boldsymbol{k}}\right)\times\hat{\boldsymbol{k}}\right], \tag{8.1}$$

https://doi.org/10.1017/S0022377824001272 Published online by Cambridge University Press

where $M^2(=\sigma_1 \boldsymbol{B}_0^2 d^2/\epsilon\rho_m\nu)$ is the Hartmann number, which accounts for the effect of the magnetic field. Here, σ_1 is the electrical conductivity.

The eigenvalue problem for nonlinear analysis incorporating the effect of magnetic field is

$$\frac{\sqrt{Ra}}{\sqrt{\lambda}}\left[\lambda+\frac{G-1}{G}\right]a^2\Theta+2\left(D^2-a^2\right)W-2\widetilde{Da}\left(D^2-a^2\right)^2W+\frac{2M^2\widetilde{Da}}{Vr}D^2W=0, \tag{8.2}$$

$$\frac{\sqrt{Ra}}{\sqrt{\lambda}}\left[\lambda+\frac{G-1}{G}\right]W+2\left(D^2-a^2\right)\Theta-2\mathcal{H}\left(\Theta-\Psi\right)=0, \tag{8.3}$$

$$\frac{2}{\gamma}\left(D^2-a^2\right)\Psi+2\mathcal{H}\left(\Theta-\Psi\right)=0. \tag{8.4}$$

The eigenvalue problem for linear analysis incorporating the effect of magnetic field is

$$\sqrt{Ra}a^2\Theta+\left(D^2-a^2\right)W-\widetilde{Da}\left(D^2-a^2\right)^2W+\frac{M^2\widetilde{Da}}{Vr}D^2W=0, \tag{8.5}$$

$$\left(D^2-a^2\right)\Theta+\mathcal{H}\left(\Psi-\Theta\right)+\sqrt{Ra}\left(1-\frac{1}{G}\right)W=0, \tag{8.6}$$

$$\left(D^2-a^2\right)\Psi-\mathcal{H}\gamma\left(\Psi-\Theta\right)=0. \tag{8.7}$$

The BCs associated with both eigenvalue problems remain the same as (4.25).

The Rayleigh–Darcy numbers for both nonlinear and linear analyses were determined by solving the eigenvalue problems using the Galerkin method as detailed in § 6. The value of Ra for nonlinear analysis has been a function of a, λ, $\mathcal{H}$, γ, M^2 and G. The optimal value of λ is $(G-1)/G$ for all combinations of bounding surfaces. Using this value of λ, we have found that Ra for nonlinear analysis has been the same as Ra for linear analysis. The Rayleigh–Darcy numbers (Ra) for distinct combinations of bounding surfaces are as follows.

For free–free bounding surfaces

$$Ra=\left(\frac{G}{G-1}\right)\frac{\left(a^2+\pi^2\right)\left(a^2+\pi^2+\left(a^2+\pi^2\right)^2\widetilde{Da}+\pi^2\widetilde{Da}M^2\right)\left(a^2+\pi^2+\mathcal{H}+\gamma\mathcal{H}\right)}{a^2\left(a^2+\pi^2+\gamma\mathcal{H}\right)}. \tag{8.8}$$

For rigid–free bounding surfaces

$$Ra=\frac{28G\left(10+a^2\right)\left(10+a^2+\mathcal{H}+\gamma\mathcal{H}\right)}{507a^2\left(G-1\right)\left(10+a^2+\gamma\mathcal{H}\right)}\times\left[19a^4\widetilde{Da}+216\left(1+21\widetilde{Da}\right)+a^2\left(19+432\widetilde{Da}\right)+216\widetilde{Da}M^2\right]. \tag{8.9}$$

For rigid–rigid bounding surfaces

$$Ra=\frac{28G\left(10+a^2\right)\left(10+a^2+\mathcal{H}+\gamma\mathcal{H}\right)}{27a^2\left(G-1\right)\left(10+a^2+\gamma\mathcal{H}\right)}\times\left[12+504\widetilde{Da}+a^4\widetilde{Da}+a^2\left(1+24\widetilde{Da}\right)+12\widetilde{Da}M^2\right]. \tag{8.10}$$

For the limiting case of the magnetic field i.e. $M^2=0$, clearly the Rayleigh–Darcy number for the respective bounding surfaces has been the same as given in (6.6), (6.8) and (6.10).

https://doi.org/10.1017/S0022377824001272 Published online by Cambridge University Press

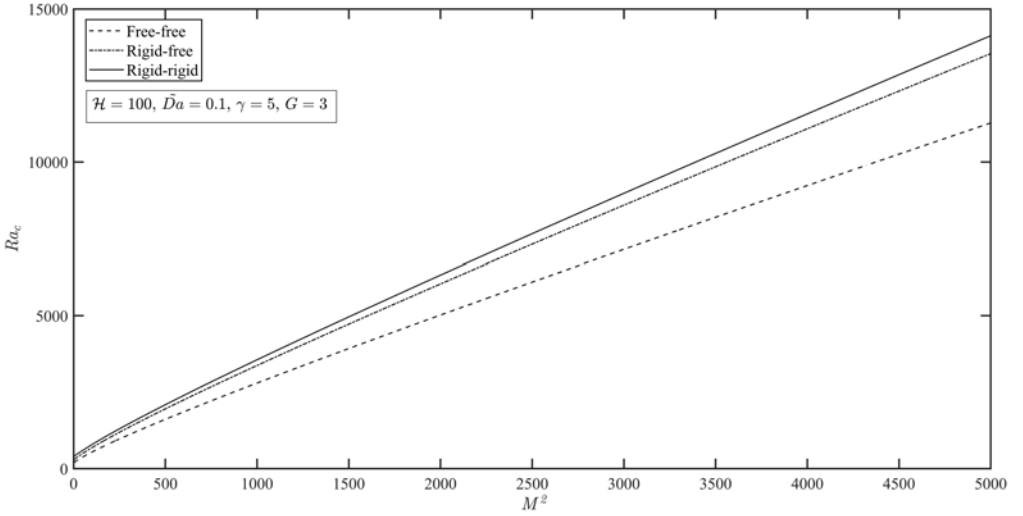

FIGURE 6. Variation of critical Rayleigh–Darcy number (Ra_c) with the square of Hartmann number (M^2) for the distinct combinations of bounding surfaces.

Figure 6 shows the variation in Ra_c with the square of the Hartmann number (M^2) for different boundary surface combinations. The figure shows that, with the increase in M^2, Ra_c also increases, indicating that magnetic fields delay the onset of thermal convection, thus exerting a stabilizing influence. This occurs because the magnetic field impedes the motion within the PIP. When the PIP attempts convective motion, the Lorentz force generated by the magnetic field counteracts this movement, resisting the flow and suppressing convective instabilities, thereby delaying convection onset. This suppression of plasma motion is essential in postponing or preventing the onset of thermal convection. Additionally, the figure reveals that PIP confined within rigid–rigid bounding surfaces exhibits greater thermal stability compared with PIP confined within rigid–free or free–free bounding surfaces.

The stability analysis of PIP in a porous medium with LTNE effects has significant applications across various scientific and engineering domains. In astrophysics, this study enhances the understanding of stellar and planetary atmospheres, contributing to more accurate models of these complex systems. In the field of nuclear fusion, it offers insights into the stability of magnetic confinement systems, which is crucial for the development of efficient fusion reactors. The findings also aid in the design of thermal protection systems for spacecraft, ensuring their integrity during re-entry and other high-temperature conditions. Furthermore, the optimization of heat exchangers and combustion chambers in engineering applications benefits from the improved thermal stability insights provided by this study. Additionally, the study informs the development of plasma-based pollution control technologies and advances in plasma medicine, particularly in the design of stable plasma sources for medical treatments involving porous tissues or materials.

9. Conclusions

This study explored the impact of LTNE and magnetic field on the stability of PIP heated from below and saturating a porous medium. We analysed three combinations of bounding surfaces: rigid–rigid, rigid–free and free–free. The eigenvalue problems resulting from

https://doi.org/10.1017/S0022377824001272 Published online by Cambridge University Press

these configurations were numerically solved using the Galerkin method. The key findings are as follows:

(i) Energy decay was examined using the energy method, revealing that the collisional frequency and diffusivity ratios significantly influence the rate of energy decay.
(ii) The principle of exchange of stabilities was confirmed, indicating the absence of oscillatory convection modes.
(iii) Both linear and nonlinear analyses showed identical stability boundaries for all bounding surface combinations, indicating the absence of a subcritical region and the establishment of global stability.
(iv) Factors such as compressibility, medium permeability and inter-phase heat transfer were found to delay the onset of thermal convection, thereby stabilizing the system.
(v) The porosity-modified conductivity ratio exhibited a destabilizing effect on the system stability. At very low heat-transfer coefficients, the critical values were independent of the porosity-modified conductivity ratio.
(vi) The presence of a magnetic field was observed to delay the onset of thermal convection, thus exerting a stabilizing effect.
(vii) Among the bounding surface configurations, rigid–rigid surfaces provided the greatest thermal stability for confining the PIP.

Future research could explore the impact of surface tension on thermal convection in partially ionized plasma using both linear and nonlinear analyses across various bounding surface configurations. Furthermore, investigating the effects of varying ionization levels, Hall currents and finite Larmor radius on stability and convection thresholds would significantly broaden the study's scope. Additionally, the application of machine learning techniques to control Rayleigh–Bénard convection in PIP presents a promising avenue for advanced control and optimization.

Acknowledgments

The authors would like to sincerely thank the esteemed editorial board and reviewers for their invaluable comments and insightful suggestions, which have greatly enriched the quality and depth of our work.

Editor Antoine C. Bret thanks the referees for their advice in evaluating this article.

Funding

This research received no specific grant from any funding agency, commercial or not-for-profit sectors.

Declaration of interests

The authors report no conflict of interest.

REFERENCES

ARNONE, G., CAPONE, F. & GIANFRANI, J.A. 2024 Stability of penetrative convective currents in local thermal non-equilibrium. *Proc. R. Soc. Lond.* A **480** (2287), 20230820.

BALLAI, I. 2019 Linear waves in partially ionized plasmas in ionization non-equilibrium. *Front. Astron. Space Sci*. **6**, 39.

BALLESTER, J.L., *et al.* 2018 Partially ionized plasmas in astrophysics. *Space Sci. Rev*. **214** (2), 58.

BALLESTER, J.L., SOLER, R., CARBONELL, M. & TERRADAS, J. 2021 The first adiabatic exponent in a partially ionized prominence plasma: effect on the period of slow waves. *Astron. Astrophys*. **656**, A159.

BANSAL, A. & SUTHAR, O.P. 2022 A study on the effect of temperature modulation on Darcy–Bénard convection using a local thermal non-equilibrium model. *Phys. Fluids* **34** (4), 044107.

BANSAL, A. & SUTHAR, O.P. 2024 Temperature modulation effects on chaos and heat transfer in Darcy–Bénard convection using a local thermal non-equilibrium model. *Nonlinear Dyn*. **112** (18), 16475–16493.

CHANDEL, V. & SUNIL 2024 Influence of magnetic fields and bounding surface configurations on thermal convection in partially ionised plasmas: nonlinear and linear stability analyses. *Pramana – J. Phys*. **98** (3), 107.

CHANDEL, V., SUNIL & SHARMA, P. 2024 Study of global stability of rotating partially-ionized plasma saturating a porous medium. *Spec. Top. Rev. Porous Media: Intl J*. **15** (6), 27–46.

CHANDRASEKHAR, S. 1981 *Hydrodynamic and Hydromagnetic Stability*. Dover.

GALDI, G.P. & STRAUGHAN, B. 1985 Exchange of stabilities, symmetry, and nonlinear stability. *Arch. Rat. Mech. Anal*. **89** (3), 211–228.

INGHAM, D.B. & POP, I. (Ed.) 2005 *Transport Phenomena in Porous Media III*. Elsevier.

KAOTHEKAR, S. 2018 Thermal instability of partially ionized viscous plasma with Hall effect FLR corrections flowing through porous medium. *J. Porous Media* **21** (8), 679–699.

KRISHAN, V. 2022 Different representations of a partially ionized plasma. *J. Astrophys. Astron*. **43** (2), 43.

KUMAR, S., POSER, A.J., SCHÖTTLER, M., KLEINSCHMIDT, U., DIETRICH, W., WICHT, J., FRENCH, M. & REDMER, R. 2021 Ionization and transport in partially ionized multicomponent plasmas: application to atmospheres of hot Jupiters. *Phys. Rev.* E **103** (6), 063203.

KUZNETSOV, A.V. 1998 Thermal nonequilibrium forced convection in porous media. In *Transport Phenomena in Porous Media* (ed. D.B. Ingham & I. Pop), pp. 103–129. Pergamon.

MAHAJAN, A. & RAJ, M. 2024 The impact of internal heating on natural convection in a rectangular porous container. *Chin. J. Phys*. **90**, 651–663.

MAHESHWARI, S.L. & BHATIA, P.K. 1976 Frictional effects with neutrals and Rayleigh–Taylor instability of a compressible Hall plasma. *Beitr. Plasmaphys*. **16** (4), 251–261.

MALASHETTY, M.S., SWAMY, M. & HEERA, R. 2008 Double diffusive convection in a porous layer using a thermal non-equilibrium model. *Intl J. Therm. Sci*. **47** (9), 1131–1147.

MALASHETTY, M.S., SWAMY, M. & KULKARNI, S. 2007 Thermal convection in a rotating porous layer using a thermal nonequilibrium model. *Phys. Fluids* **19** (5), 054102.

NIELD, D.A. & BEJAN, A. 2013 *Convection in Porous Media*. Springer.

POSTELNICU, A. 2008 The onset of a Darcy–Brinkman convection using a thermal nonequilibrium model. Part II. *Intl J. Therm. Sci*. **47** (12), 1587–1594.

POSTELNICU, A. & REES, D.A.S. 2003 The onset of Darcy–Brinkman convection in a porous layer using a thermal nonequlibrium model-part I: stress-free boundaries. *Intl J. Energy Res*. **27** (10), 961–973.

QIN, Y. & KALONI, P.N. 1995 Nonlinear stability problem of a rotating porous layer. *Q. Appl. Maths* **53** (1), 129–142.

REES, D.A.S. & POP, I. 2005 Local thermal non-equilibrium in porous medium convection. In *Transport Phenomena in Porous Media III* (ed. D.B. Ingham & I. Pop), pp. 147–173. Elsevier.

SHARMA, R.C. 1972 Finite Larmor radius and Hall effects on thermal instability of a rotating plasma. *Phys. Fluids* **15** (10), 1822–1826.

SHARMA, R.C. & SHARMA, K.C. 1978 Thermal instability of a partially ionized plasma. *Austral. J. Phys*. **31** (2), 181–188.

SHARMA, R.C. & SHARMA, Y.D. 1989 Taylor instability of partially-ionized plasma in porous medium in the presence of variable magnetic field. *Astrophys. Space Sci*. **155** (2), 295–300.

SHARMA, R.C. & SUNIL 1995 Thermal instability of a compressible finite Larmor radius, Hall plasma in porous medium. *Phys. Plasmas* **2** (6), 1886–1892.

SHARMA, R.C. & SUNIL 1996 Thermal instability of a compressible finite-Larmor-radius Hall plasma in a porous medium. *J. Plasma Phys*. **55** (1), 35–45.

SHARMA, S., SUNIL & SHARMA, P. 2024 Stability analysis of thermosolutal convection in a rotating Navier–Stokes–Voigt fluid. *Z. Naturforsch.* A **79** (7), 689–702.

SHIVAKUMARA, I.S., LEE, J., MAMATHA, A.L. & RAVISHA, M. 2011 Boundary and thermal non-equilibrium effects on convective instability in an anisotropic porous layer. *J. Mech. Sci. Technol*. **25** (4), 911–921.

https://doi.org/10.1017/S0022377824001272 Published online by Cambridge University Press

SOLER, R. & BALLESTER, J.L. 2022 Theory of fluid instabilities in partially ionized plasmas: an overview. *Front. Astron. Space Sci*. **9**, 789083.

SPIEGEL, E.A. & VERONIS, G. 1960 On the Boussinesq approximation for a compressible fluid. *Astrophys. J*. **131**, 442–447.

STRAUGHAN, B. 2004 *The Energy Method, Stability, and Nonlinear Convection*. Springer.

STRAUGHAN, B. 2006 Global nonlinear stability in porous convection with a thermal non-equilibrium model. *Proc. R. Soc. Lond.* A **462** (2066), 409–418.

STRAUGHAN, B. 2008 *Stability and Wave Motion in Porous Media*. Springer.

SUNIL, SHARMA, P. & MAHAJAN, A. 2010 Nonlinear ferroconvection in a porous layer using a thermal nonequilibrium model. *Spec. Top. Rev. Porous Media: Intl J*. **1** (2), 105–121.

THAKUR, A., KUMAR, S. & DEVI, R. 2024 The effect of rotation on ferroconvection in the presence of couple stress forces in porous medium: a nonlinear analysis. *Eur. Phys. J. Plus* **139** (3), 236.

YADAV, D., BHARGAVA, R. & AGARWAL, G.S. 2013 Thermal instability in a nanofluid layer with a vertical magnetic field. *J. Eng. Math.* **80** (1), 147–164.

YADAV, D. & LEE, J. 2015 The effect of local thermal non-equilibrium on the onset of Brinkman convection in a nanofluid saturated rotating porous layer. *J. Nanofluids* **4** (3), 335–342.